The impact of environmental investments on green innovation: An integration of factors that increase or decrease uncertainty

Shuwang Wang

Shengquan Li

Jinya Su

Juan Li

Luyao Zhang

Accepted for publication in International Journal of Control

Extended State Observer based Nonsingular Terminal Sliding Mode Controller for a DC-DC Buck Converter with Disturbances: Theoretical analysis and experimental verification

Abstract: This paper develops a continuous nonsingular terminal sliding mode controller (NTSMC) based on extended state observer (ESO) method for a DC-DC buck converter subject to both load disturbances and input voltage variations. First, a novel modeling method based on output feedback is developed to transform the matched and mismatched disturbances caused by load resistance and input voltage variations of the DC-DC buck converter into a uniform matched total disturbance. Second, a three-order ESO is established to estimate and compensate the differential of the output voltage and the total disturbance including the load disturbances and input voltage variation. Third, a nonsingular terminal sliding mode control based on the estimated values is designed to achieve faster tracking speed and better tracking accuracy around the expected voltage. In addition, the theoretical stability of the proposed controller is analyzed in detail by a Lyapunov stability criterion. Finally, both comparative simulation and experimental results show that the proposed NTSMC-ESO controller with the novel modeling method can attenuate the input voltage variation effectively and has a better load disturbance rejection ability than the conventional reduced-order ESO based sliding mode control method.

Key words: DC-DC Buck Converter, Nonsingular Terminal Sliding Mode Control, Extended State Observer (ESO), Matched/mismatched Disturbances

1. Introduction

The DC-DC buck converters are widely used in industrial control systems as the various output voltages, such as wind energy conversion systems, photovoltaic power systems, DC motor drivers, electric vehicles systems and so on, since such a converter is a power electronic device utilized to adapt the output/input voltages between the sources and load. It is well known that the circuit of a DC-DC buck converter naturally behaves with the characteristic of nonlinearity, because the switching mode frequency of the converter should be high enough to adapt to different operating modes. Additionally, high tracking performance of the DC-DC converter is difficult to achieve due to variable circuit parameters and uncertain external loads. Thus, modelling errors caused by varieties of system parameters and external uncertainties including the changes of input voltage source and load, are deemed as two of the most devastating disturbances, which would give rise to severe adverse effects on the DC-DC converter control systems. Those natural properties of the DC-DC converter may commonly bring serious challenges on efficient and high-precision controller designed by the pioneers from the academic and industrial fields. Therefore, many kinds of control methods have been developed to significantly improve disturbance rejection ability of DC-DC converter system, such as backstepping control algorithm, adaptive control, model predictive control, robust control, sliding mode control (SMC), and so on (Salimi et al., 2013; Bahtiyar et al., 2018; Alsmadi et al., 2018; Saleem et al., 2019).

These advanced methods can actually improve the dynamical performance of the DC-DC converters from different aspects. It is also found that excellent robustness of the above control methods can be achieved by sacrificing other control performance, such as the tracking performance, fast dynamical response, etc, except the SMC and disturbance rejection/ observer based control approaches. Additionally, average model can intuitively reflect switching feature of DC-DC converter to enhance control performance (Sira-Ramirez & Rios-Bolivar, 1994; Li et al., 2017). Therefore, a linear sliding model control method based on an average model is applied to a DC-DC buck converter, since it can attenuate the effects of matched disturbances and modeling errors from model parameter uncertainties in ref. (Kumar & Gupta, 2016). An adaptive control algorithm has been applied in sliding mode control method to attenuate uncertainties and noisy signals for a bidirectional voltage converter (Cavallo et al, 2020). In order to achieve control tasks of battery charging and generator current limiting respectively, an adaptive sliding mode manifold has been used to realize each object (Canciello et al. 2021). Unfortunately, there are not only the inherent disadvantages of SMC, i.e., chattering phenomenon and sensitiveness of the mismatched disturbance, but also the excessive control energy that is generally required due to the conservative operation with a larger switching gain than the amplitude of the disturbances (Wu et al, 2017; Levant, 2003).

Non-singular terminal sliding-mode control (NTSMC) approach with a nonlinear sliding surface has been adopted for high requirement on a DC-DC buck converter (Pichan et al., 2020; Yang et al 2013; Wang et al; 2020). In this method, the time taken to reach the desired set point from any initial states under the disturbances is guaranteed to be a finite time, so output voltage in DC-DC buck converter will reach the desired voltage within time required. In addition, mismatched disturbances, which do not act in the same channel as the control input, are commonly in the form of resistance load in DC-DC buck converter systems (Wang et al, 2020). Therefore, a number of disturbance estimation technologies are proposed to improve the performance of SMC-based control method. Considering the mismatched uncertainties, a disturbance observer (DO) composite fractional-order nonsingular terminal sliding mode controller has been developed to estimate and compensate for the mismatched disturbance in an uncertain system (Razzaghian et al., 2021). In ref. (Liu et al., 2019), extended state observer (ESO) is used to estimate various uncertainties and disturbances to enhance the robustness of sliding mode technique for the polymer electrolyte membrane fuel cell air-feed system. An integral sliding mode control (ISMC)-based DOB method has been used to solve the system mismatched disturbances by introducing an integral sliding mode surface (Zhang & Liu, 2016). An uncertainty and disturbance estimator (UDE) based sliding mode control approach is applied to improve the performance of power converters with parameter uncertainties (Tian et al., 2018). The design strategy of observer-based SMC can not only conquer the challenges of SMC, but also improve the closed-loop control performance.

ESO, regarding internal and external disturbances, i.e., total disturbance, as an extended system state variable, is another effective and practical disturbance estimation and attenuation approach. The ESO-based controller, i.e., active disturbance rejection control (ADRC) method, can timely estimate both system states and total disturbance by a simple structure and computation. It can also attenuate the effect of the total disturbance via a feed-forward channel (Gao, 2014). Owing to such a promising feature, the ADRC control method has also been widely applied to industrial control fields such as permanent magnet synchronous motor (PMSM) servo system, vibration control system, and wind power system (Ran et al., 2017; Wu & Guo, 2019; Sun et al., 2018; Li et al., 2020). An ADRC method has been proposed to improve the tracking performance of a DC-DC converter with the matched disturbances in ref.

(Yang et al, 2017). The ADRC method introduced the concept of total disturbance, which represents the uncertainties and changes in system dynamics including external environmental disturbances and internal uncertainties (Huang & Xue, 2014; Zhao & Guo, 2018). Additionally, whether the internal and external disturbances are matched or mismatched, they can be lumped as the total disturbances when they affect the system output. Considering the mismatched disturbances in pulse width modulation-based DC-DC buck converter system, an enhanced sliding mode control with ESO technique is developed in refs. (Zhuo et al., 2019; Yang et al., 2017).

An ESO-based sliding mode control method has been introduced to improve performance of the controlled DC-DC buck converter system with mismatched/matched disturbances in ref. (Wang et al., 2015), but the problem of input voltage variable is not mentioned. A Finite-time disturbance observer (FTDO)-based nonsingular terminal sliding mode control (NTSMC) method has been designed to guarantee the finite-time sliding motion in the presence of mismatched disturbance (Wang et al., 2016). Above ESO-based SMC methods reveal that the essential motivation is to reject the mismatched disturbance from the perspective of controller design for DC-DC converter system. These methods can effectively solve the challenge of mismatched disturbances on the system, but will increase the design difficulty of sliding mode controller or need more sensors. In this paper, a novel method is proposed to solve the mismatched disturbances from the perspective of modeling without complicating the controller design. In addition, different from the control method proposed in (Wang et al., 2015), which needs a voltage sensor to suppress input voltage variation, the proposed method does not require this extra sensor and therefore saves costs.

To address the above control challenges in DC-DC buck converter system, all the matched disturbance and mismatched disturbance can be lumped as the total disturbance with the proposed modeling method to avoid the sensitivity of SMC to mismatched disturbance. In addition, an ESO based nonsingular terminal sliding mode control (NTSMC) method is proposed to enhance the performance by attenuating the total disturbance in this paper. The key features of the proposed strategy are as follows: (1) *A novel modeling method for DC-DC buck converter system is designed to simplify the controller and achieve better robustness, without special attention to the problem of the matched or mismatched disturbances*; (2) *This proposed method achieves faster control dynamics and higher robustness against various external uncertainties and internal disturbances*; (3) *the proposed method is simple to design and is able to save the cost of a voltage sensor*.

This remaining part of this paper is organized as follows. The output feedback mathematical model of system with matched and mismatched disturbances based on output feedback is described in Section 2. A composite ESO-based NTSMC controller is proposed in Section 3. In addition, the stability of the proposed control method will be shown in Section 4. In Section 5, both simulation and experimental results are presented to compare the proposed ESO-based NTSMC against the reduced-order ESO (RESO) based SMC for a DC-DC buck converter subject to the variations of input voltage and output load resistance. Finally, Section 5 concludes the work.

2. Mathematical model of a DC-DC buck converter

This section describes the mathematical model of a DC-DC buck converter. The circuit diagram of a DC-DC buck converter driven by PWM is shown in Fig. 1.

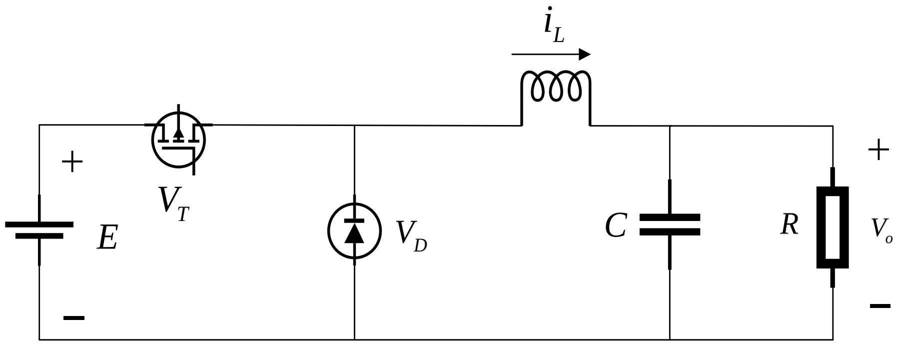

Figure 1. Average model circuit of buck converter

where E , V_T and V_D are the input voltage, the MOSFET and the circuit diode, respectively. In addition, MOSFET can be turned on and off according to the PWM wave generated by duty ratio $\mu \in [0,1]$. The circuit parameters of L , R and C represent the circuit inductance, the load resistance and the capacitance respectively. The current i_L and voltage V_o are the current flowing through the inductance and the voltage of the load resistance, i.e., the output voltage, respectively. It is assumed that the nominal values of the load resistance and input voltage are R_o and E_o respectively, because the load resistance and input voltage are both time-varying in the real industries. Therefore, the average mathematical model of a DC-DC buck converter can be deduced as follows:

$$\begin{cases} L\dot{i}_L = \mu E - V_o, \\ C\dot{V}_o = i_L - \dfrac{V_o}{R}. \end{cases} \tag{1}$$

The system mathematical model can be further rewritten as follows with the definition of $x_1 = V_o - V_r$:

$$\dot{x}_1 = \dot{e} = \frac{i_L}{C} - \frac{V_o}{R_o C} + d_1(t). \tag{2}$$

where V_r is the reference output voltage and $d_1(t) = \dfrac{V_o}{R_o C} - \dfrac{V_o}{RC}$ represents the ratio of change in load current to the capacitor. Due to the output voltage both ends of the capacitor, the current flowing through the load will not change suddenly, so $d_1(t)$ is differentiable. Output feedback modeling method has been introduced because the state variable i_L cannot be measured directly. The following equation will be deduced by define the $\dot{x}_2 = \ddot{x}_1$.

$$\begin{aligned}\dot{x}_2 &= \ddot{x}_1 \\ &= \frac{\mu E_o - V_o}{LC} - \frac{1}{R_o C}\left(\frac{i_L}{C} - \frac{V_o}{RC}\right) + \dot{d}_1(t) + d_2(t),\end{aligned} \tag{3}$$

where $d_2(t) = \dfrac{\mu(E - E_o)}{LC}$. In addition, the system modeling error caused by circuit parameter variations should also be taken into consideration to improve the control performance. Therefore, $d_3(t)$ is defined as the modeling errors of system and satisfies $d_3(t) = \dfrac{\mu E_o - V_r}{L_o C_o} - \dfrac{\mu E_o - V_r}{LC} + \dfrac{x_1}{L_o C_o} - \dfrac{x_1}{LC} + \dfrac{x_2}{R_o C_o} - \dfrac{x_2}{R_o C}$, where L_o, C_o are the nominal values of inductance and capacitance, respectively. The average mathematical model of DC-DC buck converter system can be simplified by Eq. (4):

$$\begin{cases}\dot{x}_1 = x_2 \\ \dot{x}_2 = \dfrac{\mu E_o - V_r}{L_o C_o} - \dfrac{x_1}{L_o C_o} - \dfrac{x_2}{R_o C_o} + \dot{d}_1(t) + d_2(t) + d_3(t).\end{cases} \tag{4}$$

The system model can be further reduced by Eq. (5) with $u = \dfrac{\mu E_o - V_r}{L_o C_o} - \dfrac{x_1}{L_o C_o} - \dfrac{x_2}{R_o C_o}$

$$\begin{cases}\dot{x}_1 = x_2 \\ \dot{x}_2 = u + \dot{d}_1(t) + d_2(t) + d_3(t).\end{cases} \tag{5}$$

In addition, the total disturbance D can be obtained with $D = \dot{d}_1(t) + d_2(t) + d_3(t)$:

$$\begin{cases}\dot{x}_1 = x_2 \\ \dot{x}_2 = u + D.\end{cases} \tag{6}$$

From Eq. (6) and the above analysis, the proposed modeling method does not need to distinguish the matched or mismatched disturbances, which is different from the modeling methods in ref. (Wang et al., 2015). In this way, the sensitivity of mismatched disturbance within traditional SMC can be avoided from the point of view of system modelling. The Assumption 1 is further given for the convenience of controller design and analysis.

Assumption 1: For the above DC-DC buck system, the perturbation of system parameters has been considered in this paper, if the total disturbance D does not change drastically, there exists a constant $d^* > 0$ by satisfying $d^* = \sup_{t>0} |D|$, and $\dot{D}$ is also bounded.

3. Composite controller design

3.1 *Previous method*

In ref. (Wang et al., 2015), a disturbance estimation method composited with the following SMC design procedure based on state feedback can attenuate and compensate the mismatched disturbance:

$$s = cx_1 + x_2 + z_2, \tag{7}$$

$$\begin{cases} u = -\left[c\left(x_2 + z_2\right) + \eta sgn\left(s\right)\right] + \dfrac{x_1}{LC} + \dfrac{x_2}{R_o C} - \dfrac{1}{R_o C} z_2 - \dot{z}_2 \\ \mu\left(t\right) = \dfrac{LCu + V_r}{E}. \end{cases} \tag{8}$$

The reduced order ESO (RESO) can be formulated as follows:

$$\begin{cases} \dot{z}_1 = z_2 + x_2 - \beta_1(z_1 - x_1) \\ \dot{z}_2 = -\beta_2(z_1 - x_1). \end{cases} \tag{9}$$

where z_1, z_2 are the outputs of RESO which represent the estimate value of the system state x_1 and disturbance $d_1(t)$. The parameters β_1, β_2 are defined as the gains of observer which satisfy the condition $\beta_1 > 0, \beta_2 > 0$. The RESO method in ref. (Wang et al., 2015) can also solve the input voltage disturbance, while an additional voltage sensor must be added to measure the input voltage for timely. The deviation between the nominal value and the actual value of the input voltage is defined as $\Delta E = E - E_o$. The duty ratio under input voltage disturbance is shown in Eq. (10):

$$\mu'(t) = \frac{LCu + V_r}{E_o + \Delta E}. \tag{10}$$

In this study, the composite controller is proposed to attenuate mismatched/matched disturbances of a DC-DC buck converter system without the voltage sensor in Figure 2. It is divided into two parts: one is ESO for estimating the total disturbance and system state variables, and the other one is NTSMC method for fast tracking performance.

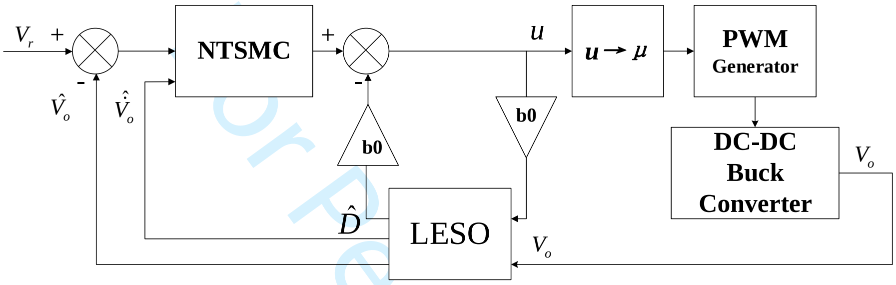

Figure 2. Control system structure of DC-DC buck converter with the proposed modeling method

3.2 *Extended state observer design*

The purpose of this section is to design a disturbance estimator for observing the total disturbances caused by input voltage and load resistance changes. According to the proposed modeling method, the DC-DC buck converter is a second-order system with total disturbance D. The total disturbance including matched and mismatched disturbances is defined as the extended state variable x_3. Therefore, a three-order linear ESO (LESO) is described by Eq. (11).

$$\begin{cases} \dot{\hat{x}}_1 = \hat{x}_2 - 3\omega(\hat{x}_1 - x_1) \\ \dot{\hat{x}}_2 = \hat{x}_3 - 3\omega^2(\hat{x}_1 - x_1) + u \\ \dot{\hat{x}}_3 = -\omega^3(\hat{x}_1 - x_1), \end{cases} \tag{11}$$

where $\hat{x}_1, \hat{x}_2$ are defined as the estimated values of system state variables, and x_3 tracks the total disturbance D. The symbol ω is the bandwidth of LESO. Both the input voltage variation and load resistance disturbances will be estimated by LESO with the proposed average model of DC-DC Buck converter. In addition, the proposed composite sliding mode-based controller is insensitive to both matched and mismatched disturbances if the total disturbances can be compensated by the feedforward channel.

3.3 *Nonsingular terminal sliding mode control design*

The proposed modeling method in this paper has an advantage that only matched disturbance exists in the whole control system, so the sliding mode controller can avoid the problem of being sensitive to mismatched disturbances. A nonsingular terminal sliding mode is proposed to achieve finite-time fast convergence property without causing any singularity problem. The sliding mode surface and control law of the NTSMC for a DC-DC system are designed by Eqs. (12)- (16).

$$s = \hat{x}_1 + \frac{1}{\beta}\hat{x}_2^{\frac{p}{q}}, \tag{12}$$

where $\beta > 0$ is a constant to be designed, and p , q are positive odd integers which satisfy the condition that $1 < p / q < 2$. Taking the time derivative of the sliding mode surface (12) along estimated values of ESO (11):

$$\dot{s} = \hat{x}_2 - 3\omega(\hat{x}_1 - x_1) + \frac{1}{\beta}\frac{p}{q}\hat{x}_2^{\frac{p}{q}-1}[\hat{x}_3 - 3\omega^2(\hat{x}_1 - x_1) + u]. \tag{13}$$

Eq. (14) is the exponential approaching rate which is selected to ensure that the system has better dynamic performance:

$$\dot{s} = -ks - \eta\,\mathrm{sgn}(s). \tag{14}$$

The parameter $\eta > 0$ is the switching gain of sign function to be designed. The control coefficient k represents the rate that system reach at the sliding mode surface. Combining Eq.

(13) with the exponential approaching rate Eq. (14), the ESO-NTSM control law can be deduced as follow:

$$u=\beta\frac{q}{p}\hat{x}_2^{1-\frac{p}{q}}\left[-\hat{x}_2+3\omega(\hat{x}_1-x_1)-ks-\eta\,\mathrm{sgn}\left(s\right)\right]-\hat{x}_3+3\omega^2(\hat{x}_1-x_1). \tag{15}$$

According to Eqs. (4)- (5), (15), the duty ratio can be deduced as follow:

$$\mu\left(t\right)=\frac{L_oC_o(u+\frac{\hat{x}_1}{L_oC_o}+\frac{\hat{x}_2}{R_oC_o})+V_r}{E_o}. \tag{16}$$

Most of the disturbances will be estimated by ESO and compensated in Eq. (15), therefore, the switching function is used to attenuate residual disturbance after ESO compensation. The rapidity of the closed-loop system can be guaranteed by selecting the appropriate k without chattering. The disturbance rejection ability can be improved by increasing the bandwidth of ESO.

Assumption 2: For the above DC-DC system, both the load disturbance and input voltage variation are constant disturbances. Therefore, the lumped disturbance D and its derivative $\dot{D}$ are supposed to be bounded.

4. Stability analysis

4.1 *Convergence analysis of ESO*

The tracking errors between the estimated values of observer and actual states of system are defined as $e_1=\hat{x}_1-x_1, e_2=\hat{x}_2-x_2, e_3=\hat{x}_3-D$, since Eq. (17) can be obtained as follows.

$$\begin{cases}\dot{e}_1=e_2-3\omega e_1\\ \dot{e}_2=e_3-3\omega^2 e_1\\ \dot{e}_3=-\omega^3 e_1-\dot{D}.\end{cases} \tag{17}$$

The Eq. (17) can be further rewritten in the following state space form:

$$\begin{bmatrix} \dot{e}_1 \\ \dot{e}_2 \\ \dot{e}_3 \end{bmatrix} = \begin{bmatrix} -3\omega & 1 & 0 \\ -3\omega^2 & 0 & 1 \\ -\omega^3 & 0 & 0 \end{bmatrix} \begin{bmatrix} e_1 \\ e_2 \\ e_3 \end{bmatrix} + \begin{bmatrix} 0 \\ 0 \\ -\dot{D} \end{bmatrix}. \tag{18}$$

The characteristic polynomial of Eq. (18) can be obtained as following Eq. (19).

$$\begin{gathered} A = \begin{bmatrix} -3\omega & 1 & 0 \\ -3\omega^2 & 0 & 1 \\ -\omega^3 & 0 & 0 \end{bmatrix}, \\ \det\left(\lambda \boldsymbol{I} - \boldsymbol{A}\right) = \lambda^3 + 3\omega\lambda^2 + 3\omega^2\lambda + \omega^3 = \left(\lambda + \omega\right)^3. \end{gathered} \tag{19}$$

where $\omega > 0$, It can be seen that if the poles of the system stay in the left-half complex plane, then the tracking errors e_1, e_2, e_3 will gradually converge to the equilibrium point $\begin{bmatrix} -\frac{\dot{D}}{\omega^3} & -\frac{3\dot{D}}{\omega^2} & -\frac{3\dot{D}}{\omega} \end{bmatrix}^{\mathrm{T}}$. According to Eq. (6), $\dot{D} = \ddot{d}_1(t) + \dot{d}_2(t) + \dot{d}_3(t)$. Since all the disturbances in this paper are considered as constant disturbances, $\dot{\mu}(t) = 0$ i.e. $\dot{d}_2(t) + \dot{d}_3(t) = 0$ when the system exists in steady states. Therefore, it can be proved that the designed observer is globally convergent.

Although LESO cannot track the system states in finite time owing to its linear nature, the tracking errors can converge to a boundary in finite time. Since the LESO is globally convergent, $|e_1|$ is monotonically decreasing and converges to zero asymptotically. It can be assumed that there exists a vicinity of $e_1 = 0$ such that for a small $L > 0$ and t_j, then $|e_1| < L$ for all $t > t_j$.

4.2 *Proof of controller stability*

The closed-loop system stability analysis consists of the DC-DC closed-loop system of Eqs. (6), (11) and (15), (16), with the following Lyapunov function:

$$V = \frac{1}{2}s^2. \tag{20}$$

Taking the derivative of Lyapunov function V based on Eq. (11), Eq. (21) can be obtained as follows:

$$
\begin{aligned}
\dot{V} &= s\dot{s} \\
&= s(\dot{\hat{x}}_1 + \frac{1}{\beta}\frac{p}{q}\hat{x}_2^{\frac{p}{q}-1}\cdot\dot{\hat{x}}_2) \\
&= s\left\{\hat{x}_2 - 3\omega(\hat{x}_1 - x_1) + \frac{1}{\beta}\frac{p}{q}\hat{x}_2^{\frac{p}{q}-1}\left[\hat{x}_3 - 3\omega^2(\hat{x}_1 - x_1) + u\right]\right\} \\
&= s\left\{\hat{x}_2 - 3\omega e_1 + \frac{1}{\beta}\frac{p}{q}\hat{x}_2^{\frac{p}{q}-1}\left[\beta\frac{q}{p}\hat{x}_2^{1-\frac{p}{q}}\left[-\hat{x}_2 + 3\omega e_1 - ks - \eta\,\mathrm{sgn}(s)\right]\right]\right\} \\
&= s\left(-ks - \eta\,\mathrm{sgn}(s)\right) \\
&= -\left(k|s| + \eta\right)|s| \\
&= -\left(k|s| + \eta\right)V^{\frac{1}{2}}.
\end{aligned}
\tag{21}
$$

It can be concluded from Eq. (21) that the system (6) will reach the nonsingular terminal sliding mode surface Eq. (12) in finite time. Define a finite time bounded (FTB) function ref. (Li & Tian, 2007) $V_1 = V + \frac{1}{2}\hat{x}_1^2 + \frac{1}{2}\hat{x}_2^2$ for the state dynamics Eq. (11) and sliding mode dynamics Eq. (21). Taking the derivative of FTB function yields:

$$
\begin{aligned}
\dot{V}_1 &= \dot{V} + \hat{x}_1\dot{\hat{x}}_1 + \hat{x}_2\dot{\hat{x}}_2 \\
&= -ks^2 - \eta|s| + \hat{x}_1(\hat{x}_2 - 3\omega e_1) + \hat{x}_2\cdot\beta\frac{q}{p}\hat{x}_2^{1-\frac{p}{q}}\left[-\hat{x}_2 + 3\omega e_1 - ks - \eta\,\mathrm{sgn}(s)\right] \\
&\le \left|-ks^2 - \eta|s| + \hat{x}_1(\hat{x}_2 - 3\omega e_1) + \hat{x}_2\cdot\beta\frac{q}{p}\hat{x}_2^{1-\frac{p}{q}}\left[-\hat{x}_2 + 3\omega e_1 - ks - \eta\,\mathrm{sgn}(s)\right]\right| \\
&\le ks^2 + \eta|s| + |\hat{x}_1||\hat{x}_2| + 3\omega|\hat{x}_1||e_1| + \beta\frac{q}{p}\left|\hat{x}_2^{2-\frac{p}{q}}\right|\left(3\omega|e_1| + k|s| + \eta + |\hat{x}_2|\right).
\end{aligned}
\tag{22}
$$

With p, q are positive odd integers and $1 < p/q < 2$, so $0 < 2 - p/q < 1$. It can be concluded that $|\hat{x}_2|^{2-\frac{p}{q}} < 1 + |\hat{x}_2|$:

$$\dot{V}_1 \le ks^2 + \eta|s| + |\hat{x}_1||\hat{x}_2| + 3\omega|\hat{x}_1||e_1| + \frac{\beta q}{p}(1+|\hat{x}_2|)[k|s| + \eta + |\hat{x}_2| + 3\omega|e_1|)]$$

$$\le 2k\frac{|s|^2}{2} + \frac{\eta^2+|s|^2}{2} + \frac{|\hat{x}_1|^2+|\hat{x}_2|^2}{2} + 3\omega\frac{|\hat{x}_1|^2+|e_1|^2}{2} + \frac{\beta q\eta}{p} + \frac{\beta q}{p}\frac{k^2+|s|^2}{2}$$

$$+\frac{q}{p}\frac{\beta^2+|\hat{x}_2|^2}{2} + \frac{3\beta q\omega}{p}|e_1| + \frac{\beta qk}{p}\frac{|s|^2+|\hat{x}_2|^2}{2} + \frac{\beta q}{p}\frac{\eta^2+|\hat{x}_2|^2}{2} + \frac{2\beta q}{p}\frac{|\hat{x}_2|^2}{2}$$

$$+\frac{3\beta q\omega}{p}\frac{|e_1|^2+|\hat{x}_2|^2}{2}$$

$$=(2k+1+\frac{\beta q}{p}+\frac{\beta qk}{p})\frac{|s|^2}{2} + (1+3\omega)\frac{|\hat{x}_1|^2}{2} + [1+(1+\beta k+2\beta+3\beta\omega)\frac{q}{p}]\frac{|\hat{x}_2|^2}{2}$$

$$+\left[\beta\eta + \frac{\beta^2}{2} + \frac{\beta k^2}{2} + \frac{\beta\eta^2}{2} + 3\beta\omega|e_1| + \frac{3\beta\omega}{2}|e_1|^2\right]\cdot\frac{q}{p} + \frac{\eta^2}{2} + \frac{3\omega}{2}|e_1|^2$$

$$\le K_{V_1}(\frac{1}{2}s^2 + \frac{1}{2}\hat{x}_1{}^2 + \frac{1}{2}\hat{x}_2{}^2) + L_{V_1}$$

$$= K_{V_1}V_1 + L_{V_1} \qquad (23)$$

where $K_{V_1} = \max\{2k+1+\frac{\beta q}{p}+\frac{\beta qk}{p}, 1+3\omega, 1+(1+\beta k+2\beta+3\beta\omega)\frac{q}{p}\} > 0$ and $L_{V_1} = \left[\beta\eta + \frac{\beta^2}{2} + \frac{\beta k^2}{2} + \frac{\beta\eta^2}{2} + 3\beta\omega|e_1| + \frac{3\beta\omega}{2}|e_1|^2\right]\cdot\frac{q}{p} + \frac{\eta^2}{2} + \frac{3\omega}{2}|e_1|^2 > 0$ are bounded constants due to the boundedness of e_1. In Eq. (23), since $K_{V_1} > 0$ and $L_{V_1} > 0$ one can obtain that $\psi(V_1) = L_{V_1}V_1 + K_{V_1}$ is a non-decreasing function of V_1 and satisfies the following conditions for some constant $a > 0$, $\psi(a) > 0$ and $\int_a^\infty \frac{d\tau}{\psi(\tau)} = \infty$. It is also noted that $V_1 = \rho(x) = \frac{1}{2}(s^2 + \hat{x}_1{}^2 + \hat{x}_2{}^2) \ge 0$ with $x = [s \quad \hat{x}_1 \quad \hat{x}_2]^{\mathrm{T}}$ is continuous and satisfies $\lim_{\|x\|\to\infty}\rho(x) = \infty$. So V_1 is positive, definite, proper, radially unbounded and decrescent (see, the definition of decrescent in Section 2.1 of (Li, S. H., & Tian, Y. P. (2007)). So it satisfies the conditions of finite-time bounded (FTB) function of Assumption 3 of Li, S. H., & Tian, Y. P. (2007). Therefore, it follows from Lemma 1 and Section 3.2 (the two lines after Eq. (14)) of Li, S. H., & Tian, Y. P. (2007) that $\dot{V} \le L_{V_1}V_1 + K_{V_1}$ implies that V_1 and so $s, \hat{x}_1, \hat{x}_2$ will not escape to infinity in a finite time. A similar proof is also available in Theorem 1 (Eq. (18)) of (Yang, J., Su, J.Y., li, S. H., & Yu, X. H. (2014)) and Theorem 1 (Eq. (11)) of (Yang, J., Li, S. H., & Yu, X. H. (2013)).

As a result, this proves the stability of the overall control system in any finite time (including the convergence period of the observer) and so after the convergence of the observer (in steady state), sliding mode surface (12) will reduce to with certain accuracy (depending on the observer error):

$$s = x_1 + \frac{1}{\beta} x_2^{\frac{p}{q}}. \tag{24}$$

It can be found from above that system states will converge to a subdomain of estimate errors. Due to the constant disturbance considered in this paper, the state estimation error of ESO disappears, and the tracking error of the system can converge to zero in a finite time (with certain accuracy) when ESO exists in a steady state shown in Figure 3 $t = 0.22$. The time when the system state variables enter into a steady state is defined as t_r, and the sliding motion is described as:

$$s = x_1 + \frac{1}{\beta} x_2^{\frac{p}{q}} = 0. \tag{25}$$

The time of the system state variables converging to the equilibrium point t_s can be obtained by the following equation:

$$\frac{dx_1}{dt} = -\beta^{\frac{q}{p}} x_1^{\frac{q}{p}}. \tag{26}$$

The following equation can be deduced by integrating Eq. (26):

$$\int_{x_1(t_r)}^{0} x_1^{-\frac{q}{p}} dx_1 = -\beta^{\frac{q}{p}} \int_{t_r}^{t_s + t_r} dt, \tag{27}$$

where the time constants t_s and t_r satisfy the following relationship:

$$t_s = \frac{p}{\beta^{\frac{q}{p}}(p-q)} |x_1(t_r)|^{\frac{p-q}{p}}. \tag{28}$$

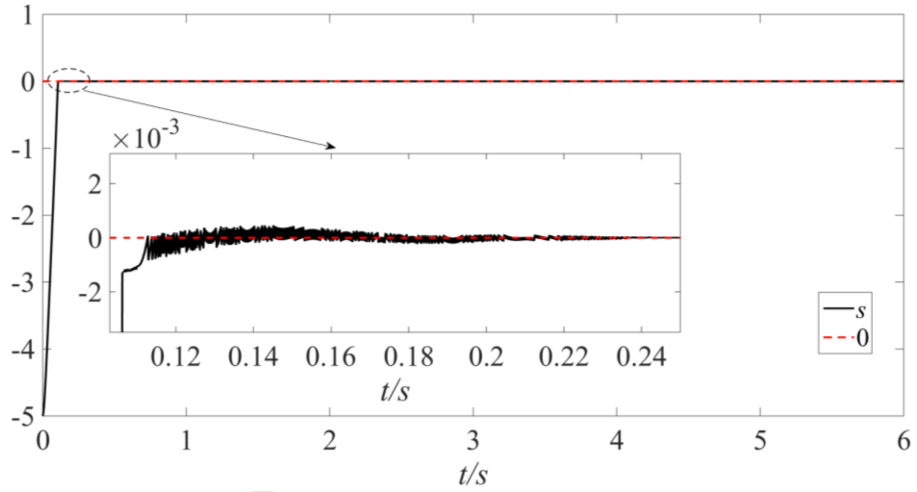

Figure 3. The trajectory of sliding mode surface $s = 0$

The above proof implies that states of DC-DC buck system can be driven to the desired equilibrium point and the control law can force the DC-DC system states to reach the sliding-mode surface in a finite time. Appropriate parameters β, p, q are selected to satisfy the actual requirements.

Remark 1: The parameter selection criterion of ESO-NTSMC controller is as follows: The gain of the nonsingular sliding mode surface β is a positive constant. The larger the β is, the faster the output voltage converges. The parameters p, q are odd numbers and satisfy $1 < p/q < 2$. In addition, the closer the term of p/q approaches to 2, the faster the system convergences. As long as the bandwidth $\omega > 0$, the LESO is global convergent. The tracking speed of state variables and the disturbance rejection ability can be improved by increasing ω. In addition, large bandwidth of LESO will amplify the measurement noise of the voltage sensor. The two parameters of exponential approaching rate $k > 0, \eta > 0$ are the approaching speed and the switching gain respectively. The convergence speed can be improved by increasing k, and the disturbance rejection ability can be improved by increasing η. Usually the switching gain η of NTSMC is larger but higher values of switching gain may cause chattering phenomenon in control system.

5. Simulation and experiment results

5.1 *Numerical simulation*

The simulation verification is based on MATLAB/ SIMULINK with the proposed average mathematical model in this paper. The desired output voltage value and the circuit parameters of DC-DC buck converter are shown in Table 1. To compare the disturbance rejection ability of RESO-SMC and ESO-NTSMC methods, two different types of disturbances similar as the actual DC-DC converter have been studied in this section. One is the load resistance change, and the other is input voltage variation. The load resistance changes from 300Ω to 400Ω and then to 250Ω at 2s and 4s. In addition, the input voltage variations are set to change from 10V to 9V and then to 10.5V at 2s and 4s respectively.

Table 1. Parameters of the DC-DC buck converter

Parameters	Symbol	Value
Input voltage	E	10V
Reference voltage	V_r	5V
Inductance	L	0.1mH
Capacitance	C	4.7μF
Load resistance	R	300Ω

To have a fair comparison, appropriate parameters have been chosen for SMC-RESO in Eqs.

(9)- (11) and ESO-NTSMC in Eqs. (13)- (18) with the satisfactory dynamic performance. Under the load resistance disturbances, the parameters in RESO-SMC controller are selected as $c = 10$, $\beta_1 = 800$, $\beta_2 = 160000$ and $\eta = 6000$, while the parameters of ESO-NTSMC controller are selected as $p = 5, q = 3$, $\beta = 20, \omega = 800, k = 5$ and $\eta = 100$. When the controllers are used in system with input voltage variations, the parameters are selected as follow: RESO-SMC: $c = 1000, \beta_1 = 1200, \beta_2 = 360000$ and $\eta = 8000$; ESO-NTSMC: $p = 5, q = 3, \beta = 1200$, $\omega = 600, k = 10$ and $\eta = 250$. The response curves subject to the two kinds of disturbances are shown in Figs 5 and 6, respectively.

Comparing the simulation results in Figure 4, it can be observed that the voltage value of ESO-NTSMC controller changed 0.2V less than the RESO-SMC controller and the settling time of the ESO-NTSMC controller is 0.1s faster than the RESO-SMC controller when the load resistances change. It can be concluded that the ESO-NTSMC controller has better load disturbance rejection ability than the RESO-SMC controller.

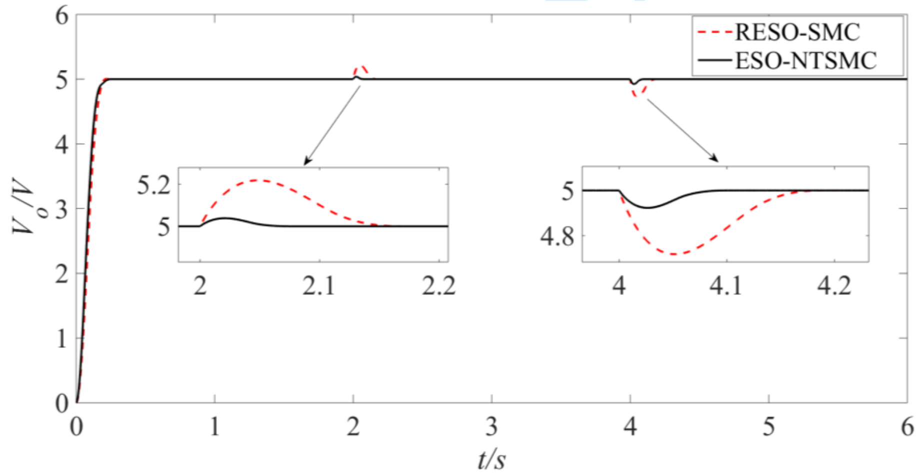

(a)

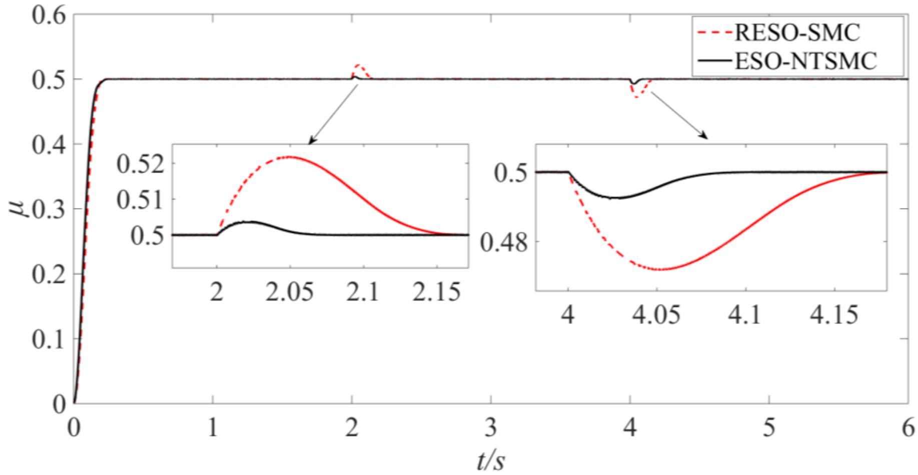

(b)

Figure 4. Response curves under ESO-NTSMC controller and RESO-SMC controller when the load resistance is changed.

(a) Output voltage V_o; (b) Duty ratio μ

It is shown in Figure 5 that the ESO-NTSMC controller has overshoot when two controllers have a similar rapidity. Although the ESO-NTSMC controller changes large in the presence of input voltage variation, it will return to the steady state within 0.02s. However, the RESO-SMC controller cannot attenuate the input voltage variation as shown in Figure 5. This is because the RESO can only be used to estimate the mismatched disturbance $d_1(t)$ while the disturbance caused by input voltage changes in Eq. (12) cannot be estimated. The closed-loop system is stable only when the switching gain is greater than the input voltage disturbance $d_2(t)$. However, a large chattering produced by a large switching gain will affect the steady-state system characteristics. Therefore, the RESO-SMC method cannot achieve satisfying control performance under input voltage variations. By using the modeling method proposed in this paper, all the disturbances that affect the output voltage will be estimated and compensated by ESO. The input voltage disturbance caused by Eq. (12) will be observed and compensated, therefore, the problem of input voltage ripple of buck converter can be solved well, which reduces the filter requirements and increases the accuracy of the current sensing for better performance and efficiency of converter.

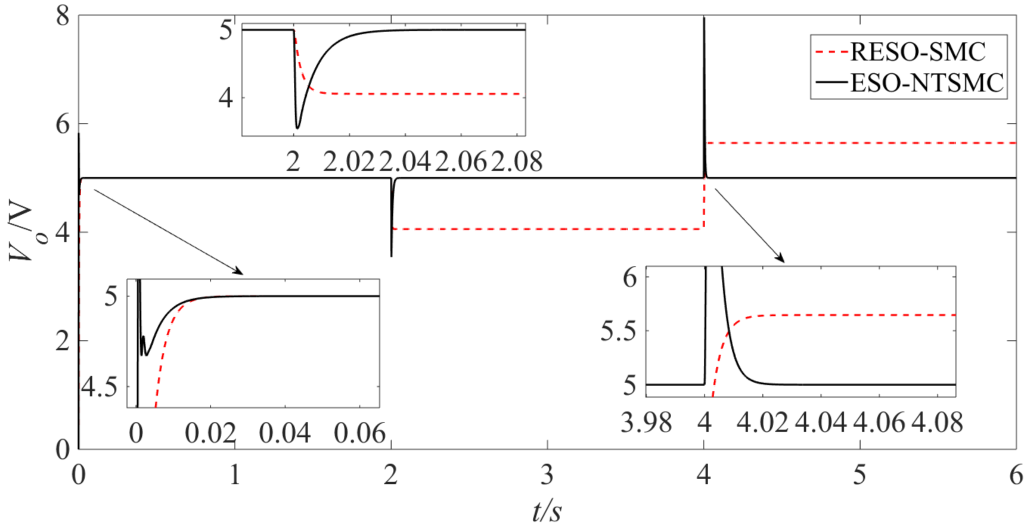

(a)

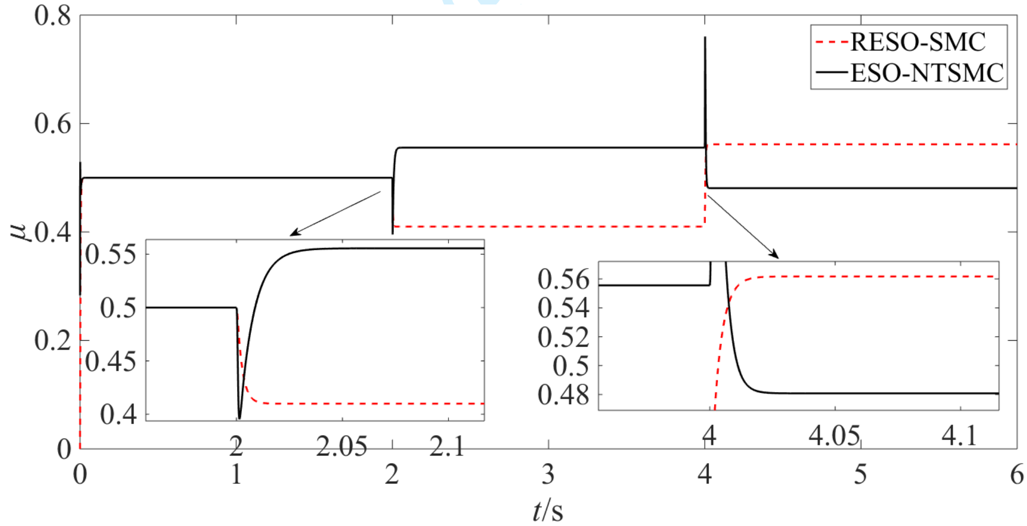

(b)

Figure 5. Response curves under ESO-NTSMC controller and RESO-SMC controller when the input voltage is varied.

(a) Output voltage V_o; (b) Duty ratio μ

5.2 *Experiment results*

To verify the disturbance rejection ability of the proposed ESO-NTSMC controller, experimental results are also presented between Eq. (10) and Eq. (17). The experiment test system of DC-DC Buck converter is shown in Figure 6. It can be found from Figure 6 that the DC-DC buck converter of the experiment is composed of three parts: the converter circuit, the programmable DC electronic load and DC power supply. The programmable DC electronic load and DC power supply from ITECH company can be used to achieve precise values and simulate the disturbance in real industries by programming in the master computer on the left. The designed control algorithm will be realized in the PC LabVIEW by graphical programming language. Then the control algorithm will be compiled into the real-time National Instrument's compact-RIO (CRIO) control board, which is composed of the FPGA and ARM chip. Analog input and output module cards are inserted into the CRIO card slots. During the experiment, the analog input card will collect the output voltage at both ends of the DC electronic load firstly; Then the appropriate duty ratio will be calculated according to the compiled algorithm; Finally, the PWM wave will be generated according to duty ratio and output by the analog output card. The output voltage of the converter will meet the requirement by driving the MOSFET on and off through PWM wave.

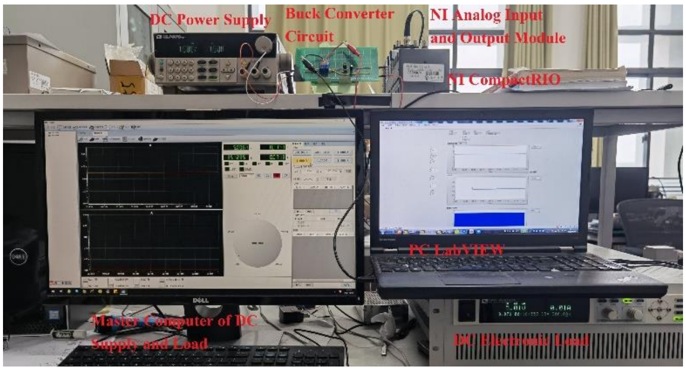

Figure 6. Experimental test system setup of the DC-DC buck converter system

Two kinds of disturbances are taken into consideration in the experiment, including the load disturbances changing from 300 Ω to 400 Ω at 30s, and from 400 Ω to 250 Ω at 60s; and the input voltage dropping from 10V to 9V at 30s, and rising from 9V to 10.5V at 60s. To compare the disturbance rejection ability, the transition time of two controllers have been adjusted the same artificially by choosing appropriate parameters. In system (8), the parameters of RESO-SMC controller are chosen as $c = 200, \eta = 20000, \beta_1 = 600$, $\beta_2 = 90000$, and the control parameters of ESO-NTSMC controller are selected as $\beta = 200,\ p = 5, q = 3, k = 200,\quad \eta = 100, \omega = 300$.

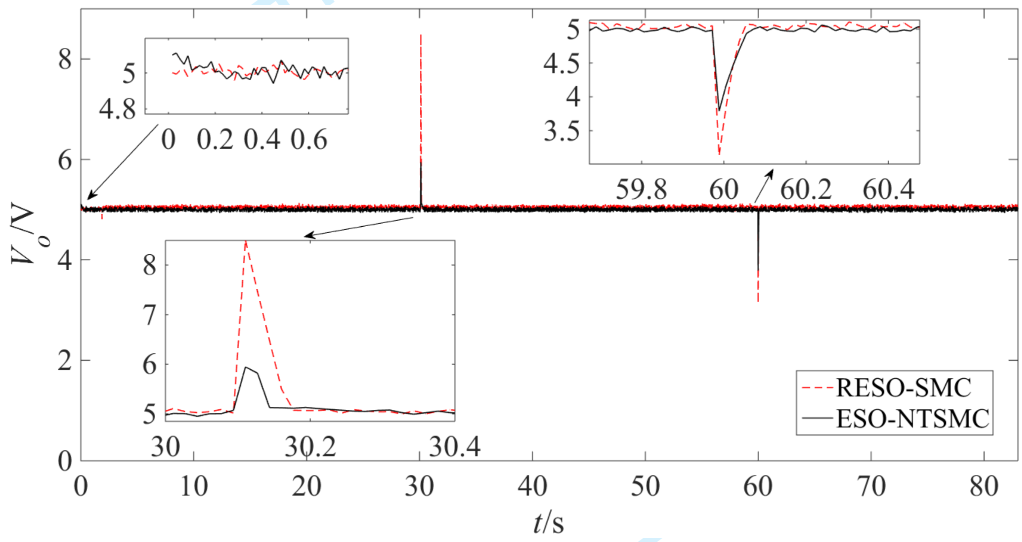

(a)

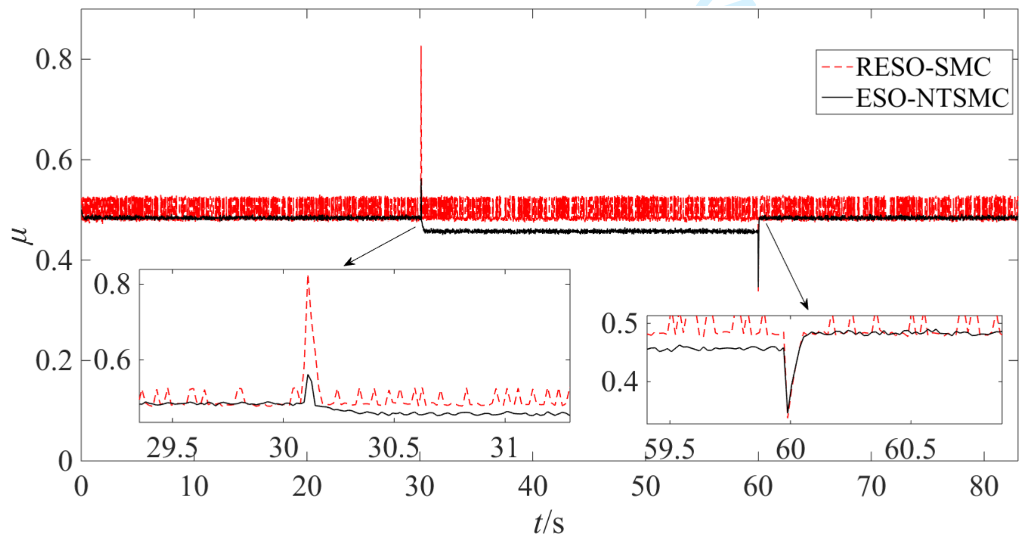

(b)

Figure 7. Response curves under ESO-NTSMC controller and RESO-SMC controller when load resistance changed

(a) Output voltage V_o; (b) Duty ratio μ

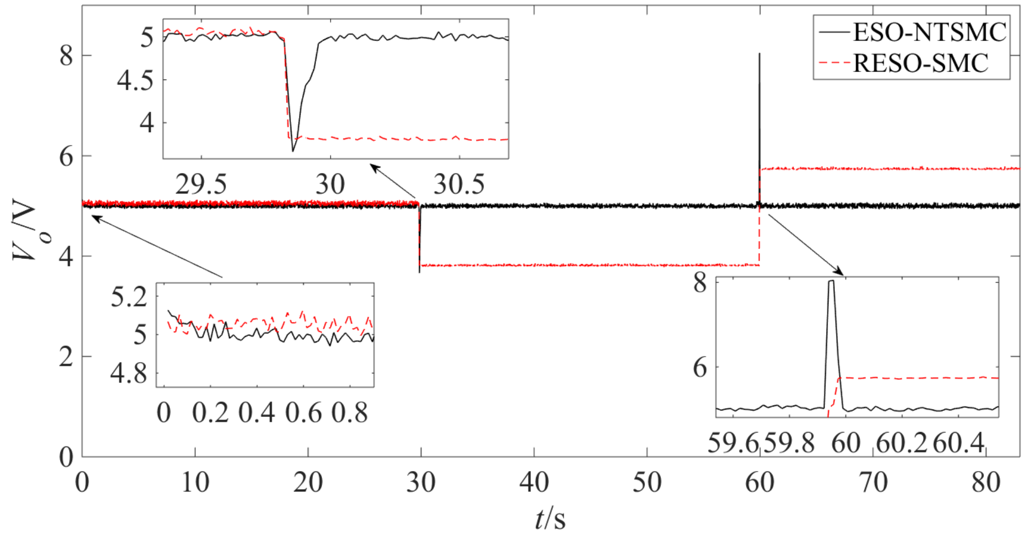

(a)

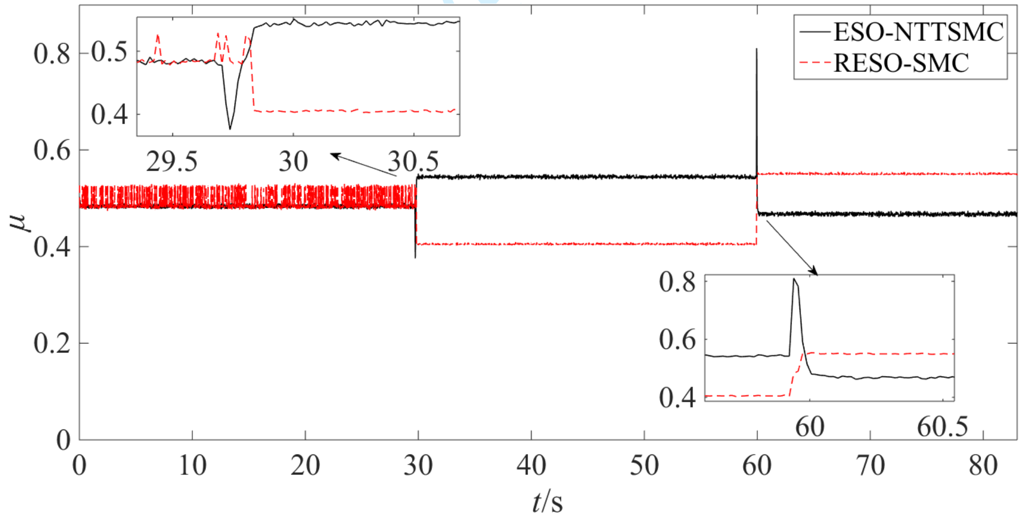

(b)

Figure 8. Response curves under ESO-NTSMC controller and RESO-SMC controller when input voltage changed

(a) Output voltage V_o; (b) Duty ratio μ

In Figure 7 and Figure 8, the black solid lines are used to represent the response curves under

ESO-NTSMC controller, and the red dotted lines are under RESO-SMC controller. It is shown in Figure 8 that the output voltage under RESO-SMC controller will increase to 8.4V when the load resistance changes at 30s and return to 5V after 0.1s. However, the output voltage under ESO-NTSMC controller only increased 1V and returned to a steady state after 0.05s. The RESO-SMC controller and ESO-NTSMC controller has a similar converge time when the load resistance decreases at 60s, but the output voltage variation of ESO-NTSMC controller is 0.8V less than that of RESO-SMC controller. Figure 8 shows the dynamic performance of the system under input voltage variation. It can be found that the experimental results are similar to the simulation results: the ESO-NTSMC controller can attenuate the input voltage disturbances effectively while the RESO-SMC controller cannot. Combining Figure 7(a) with Figure 8(a), it is observed that the ESO-NTSMC controller has overshoot which is the same as the simulation results. It can also be concluded from Figure 7(b) and Figure 8(b) that RESO-SMC controller has a larger chattering phenomenon than ESO-NTSMC controller. This is because most disturbances of DC-DC buck converter in ESO-NTSMC controller have been compensated by ESO, while RESO-SMC controller uses switching function to suppress most disturbances. Therefore, the ESO-NTSMC controller based on the novel modeling method can attenuate disturbances effectively and reduce chattering phenomenon.

6. Conclusions

In this paper, a novel modeling method is proposed to transform the mismatched and matched disturbance into a matched total disturbance. Based on the novel modeling method, an ESO-NTSMC controller is applied for the DC-DC buck converter system with load disturbances and input voltage variations. Both numerical simulation and experiments are conducted to compare the control performance between ESO-NTSMC controller and RESO-SMC controller. It has been found that the ESO-NTSMC controller has a better load disturbance rejection ability and is able to attenuate the input voltage variation effectively with little chattering.

Acknowledgements

List of abbreviations and symbols

Abbreviations

NTSMC	nonsingular terminal sliding mode control
ESO	extended state observer
SMC	sliding mode control
ADRC	active disturbance rejection control
RESO	reduced order extended state observer

Variables

L	circuit inductor
C	circuit capacitor
R	circuit resistance
E	input voltage
R_o	nominal value of circuit resistance
E_o	nominal value of input voltage
i_L	current flowing through the inductor

V_o	output voltage
μ	duty ratio
V_r	expect output voltage
x_1	tracking error of output voltage
x_2	first-order derivative of track error
u	control input
D	total disturbance
b_0	constant control gain
z_1, z_2	states of RESO
β_1, β_2	gains of RESO
c	sliding mode surface gain
η	switching gain of SMC
$\hat{x}_1, \hat{x}_2, \hat{x}_3$	states of LESO
e_1, e_2, e_3	tracking errors of LESO
ω	bandwidth of LESO
β	gain of nonsingular terminal sliding mode surface
p, q	positive odd integers
η'	switching gain of NTSMC

References

Cavallo, A., Canciello, G., & Russo, A. (2020). Integrated supervised adaptive control for the more Electric Aircraft. *Automatica*, 117, DOI: 10.1016/j.automatica.2020.108956.

Alsmadi, Yazan, M., Utkin, V., Haj-ahmed, & Mohammed. A. (2018). Sliding mode control of power converters: DC/DC converters. *International Journal of Control,* 91 (11): 2472-2493.

Bahtiyar, B., Cetin, M., & Beyhan, S. (2018). An efficient sliding mode observer-based model predictive control: experimental implementation on a DC/DC power converter. *Transactions of the Institute of Measurement and Control,* 40 (8): 2488-2497.

Gao, Z. Q. (2014). On the centrality of disturbance rejection in automatic control. *ISA Transactions,* 53 (4): 850–857.

Canciello, G., Cavallo, A., Lo Schiavo, A., & Russo, A. (2020). Multi-objective adaptive sliding manifold control for More Electric Aircraft. *ISA Transactions,* 107: 316-328.

Huang, Y., & Xue, W. C. (2014). Active disturbance rejection control: Methodology and theoretical analysis. *ISA Transactions,* 53: 963-976.

Kumar, M., & Gupta, R. (2016). Stability and sensitivity analysis of uniformly sampled DC–DC converter with circuit parasites. *IEEE Transactions on Circuits and Systems,* 63 (11): 2086-2097.

Levant, A. (2003). Higher-order sliding modes, differentiation and output-feedback control. *International Journal of Control,* 76 (9-10): 924-941.

Li, S. H., & Tian, Y. P. (2007). Finite-time stability of cascaded time-varying systems. *International Journal of Control,* 80 (4): 646-657.

Li, S. Q., Zhu, C. W., & Mao, Q. B. (2020). Active disturbance rejection vibration control for all-clamped piezoelectric plate with delay. *Control Engineering Practice,* 108, DOI: 10.1016/j.conengprac.2020.104719.

Li, Z. J., Xie, X. J., & Zhang, K. M. (2017). Output feedback stabilisation for nonlinear systems with unknown output function and control coefficients and its application. *International*

Journal of Control, 90 (5): 1027-1036.

Liu, J. X., Gao, Y. B., & Su, X. J. (2019). Disturbance-observer-based control for air management of PEM fuel cell systems via sliding mode technique, *IEEE Tractions on Control Systems Technology, 27 (3):* 1129-1138.

Pichan, M., Markadeh, G. A., & Blaabjerg, F. (2020). Continuous finite-time control of four-leg inverter through fast terminal sliding mode control. *International Transactions on Electrical Energy System, 30 (6):* 1-12.

Ran, M. P., Wang, Q., & Dong, C. Y. (2017). Active disturbance rejection control for uncertain nonaffine-in-control nonlinear systems. *IEEE Transactions on Automatic Control, 62 (11):* 5830-5836.

Razzaghian, A., Moghaddam, R. K., & Pariz, N. (2021). Fractional-order nonsingular terminal sliding mode control via a disturbance observer for a class of nonlinear systems with mismatched disturbances. *Journal of Vibration and Control, 27 (1):* 140-151.

Saleem, O., Shami, U.T., & Mahmood-ul-Hasan, K. (2019). Time-optimal control of DC-DC buck converter using single-input fuzzy augmented fractional-order PI controller. *International Transactions on Electrical Energy System, 29 (10):* 1-20.

Salimi, M. J., Soltani, G.A., Markdehi, N. R., & Abjadi. (2013). Adaptive nonlinear control of the DC-DC buck converters operating in CCM and DCM. *International Transactions on Electrical Energy System, 23 (8):* 1536-1547.

Sira-Ramirez, H., & Rios-Bolivar, M. (1994). Sliding mode control of DC-to-DC power converters via extended linearization. *IEEE Transactions on Circuits and Systems I: Fundamental Theory and Applications, 41 (10):* 652-661.

Sun, Z. X., Li, S. H., Wang, J.G., & Zhang, X. H. (2018). Adaptive composite control method of permanent magnet synchronous motor systems'. *Transactions of the Institute of Measurement and Control,* 40 (11): 3345-3357.

Tian, Z., Liu, Z. Y., Yuan, J.Q., & Wang, C. (2018). UDE-based sliding mode control of DC-DC power converters with uncertainties. *Control Engineering Practice,* 83: 116-128.

Wu, L. G., Gao, Y. X., Liu, J. X., & Li, H. Y. (2017). Event-triggered sliding mode control of stochastic systems via output feedback. *Automatica,* 82: 79-92.

Wu, Z. H., & Guo, B. Z. (2019). On convergence of active disturbance rejection control for a class of uncertain stochastic nonlinear systems. *International Journal of Control,* 92(5): 1103-1116.

Wang, J. X., Li, S. H., Yang, J., Wu, B., & Li, Q. (2015). Extended state observer-based sliding mode control for PWM-based DC–DC buck power converter systems with mismatched disturbances. *IET Control Theory and Applications,* 9 (4): 579-586.

Wang, J. X., Li, S. H., Yang, J., Wu, B., & Li, Q. (2016). Finite-time disturbance observer based nonsingular terminal sliding mode control for PWM-based DC-DC buck converters with mismatched Load Disturbances. *IET Power Electronics,* 1-20.

Wang, J. X., Rong, J. Y., & Yu, L. (2020). Reduced-order extended state observer based event-triggered sliding mode control for DC-DC buck converter system with parameter perturbation. *Asian Journal of Control,* 10: 1-11.

Wang, Z., Li, S. H., & Li, Q. (2020). Discrete-time fast terminal sliding mode control design for DC-DC buck converters with mismatched disturbances. *IEEE Transactions on Industrial Informatics,* 16 (2): 1204-1213.

Yang, J., Cui, H. Y., & Li, S. H. (2017). Optimized active disturbance rejection control for DC-DC buck converters with uncertainties using a reduced-order GPI observer. *IEEE Transaction on Circuits and Systems,* 9: 1549-8328.

Yang, J., Li, S. H., & Yu, X. H. (2013). Continuous nonsingular terminal sliding mode control for systems with mismatched disturbances. *Automatica,* 49: 2287-2291.

Yang, J., Su, J.Y., Li, S. H., & Yu, X. H. (2014). High-order Mismatched disturbance compensation for motion control systems via a continuous dynamic sliding-mode approach. IEEE Transactions on Industrial Informatics, 10 (1): 1551-3203.

Zhang, J. H., & Liu, X. W. (2016). Disturbance observer-based integral sliding-mode control for systems with mismatched disturbances. *IEEE Transactions on Industrial Electronics,* 63 (11): 7040-7048.

Zhao, Z. L., & Guo, B. Z. (2018). A novel extended state observer for output tracking of MIMO systems with mismatched uncertainty. *IEEE Transactions on Automatic Control,* 63 (1): 211-218.

Zhuo, S. R., Gaillard, A., Guo, L., & Xu, L. C. (2019). Active disturbance rejection voltage control of a floating interleaved DC-DC boost converter with switch fault consideration. *IEEE Transactions on Power Electronics,* 34 (12): 12396-12409.